J Neurophysiol 100: 371–384, 2008.
First published May 14, 2008; doi:10.1152/jn.00062.2008.

Intrinsic and Extrinsic Light Responses in Melanopsin-Expressing Ganglion Cells During Mouse Development

Tiffany M. Schmidt, Kenichiro Taniguchi, and Paulo Kofuji
Department of Neuroscience, University of Minnesota, Minneapolis, Minnesota

Submitted 17 January 2008; accepted in final form 14 May 2008

Schmidt TM, Taniguchi K, Kofuji P. Intrinsic and extrinsic light responses in melanopsin-expressing ganglion cells during mouse development. *J Neurophysiol* 100: 371–384, 2008. First published May 14, 2008; doi:10.1152/jn.00062.2008. Melanopsin (Opn4) is a photopigment found in a subset of retinal ganglion cells (RGCs) that project to various brain areas. These neurons are intrinsically photosensitive (ipRGCs) and are implicated in nonimage-forming responses to environmental light such as the pupillary light reflex and circadian entrainment. Recent evidence indicates that ipRGCs respond to light at birth, but questions remain as to whether and when they undergo significant functional changes. We used bacterial artificial chromosome transgenesis to engineer a mouse line in which enhanced green fluorescent protein (EGFP) is expressed under the control of the melanopsin promoter. Double immunolabeling for EGFP and melanopsin demonstrates their colocalization in ganglion cells of mutant mouse retinas. Electrophysiological recordings of ipRGCs in neonatal mice (postnatal day 0 [P0] to P7) demonstrated that these cells responded to light with small and sluggish depolarization. However, starting at P11 we observed ipRGCs that responded to light with a larger and faster onset (<1 s) and offset (<1 s) depolarization. These faster, larger depolarizations were observed in most ipRGCs by early adult ages. However, on application of a cocktail of synaptic blockers, we found that all cells responded to light with slow onset (>2.5 s) and offset (>10 s) depolarization, revealing the intrinsic, melanopsin-mediated light responses. The extrinsic, cone/rod influence on ipRGCs correlates with their extensive dendritic stratification in the inner plexiform layer. Collectively, these results demonstrate that ipRGCs make use of melanopsin for phototransduction before eye opening and that these cells further integrate signals derived from the outer retina as the retina matures.

INTRODUCTION

Many aspects of behavior and physiology exhibit daily oscillations known as circadian rhythms (Hastings et al. 2003; Herzog 2007). In mammals, circadian rhythms are driven by a biological clock found in the suprachiasmatic nuclei (SCN) (Hastings and Herzog 2004; Maywood et al. 2006). These intrinsic circadian rhythms are synchronized to the environmental cycle of day and night by the process of photoentrainment, which uses environmental light information to entrain the biological clock. In mammals, the signal for photoentrainment arises from a subset of retinal ganglion cells (RGCs) that send projections to the SCN. These ganglion cells that project to the SCN express melanopsin and are intrinsically photosensitive (ipRGCs) (Berson et al. 2002; Hattar et al. 2002). The sensitivity, spectral tuning, and slow kinetics of these ipRGCs closely match those of the photic entrainment mechanism, suggesting that these ganglion cells form the primary pathway for circadian entrainment (Berson 2007; Fu et al. 2005a,b; Kumbalasiri and Provencio 2005; Peirson and Foster 2006).

Furthermore, there is evidence that ipRGCs are capable of phototransduction in newborn mice when rods and cones are not yet formed (Hannibal and Fahrenkrug 2004; Sekaran et al. 2005). Calcium imaging and multielectrode array recordings from wild-type and melanopsin-null mouse retinas suggest that ipRGCs are photosensitive at early postnatal stages (postnatal day 0 [P0] to P5) (Sekaran et al. 2005; Tu et al. 2005). Light-evoked Fos induction in the SCN of mice can be detected as early as P0 (Hannibal and Fahrenkrug 2004; Lupi et al. 2006), indicating that ipRGCs are the first functional photosensitive cells in the retina.

Although ipRGCs respond to light via melanopsin-mediated phototransduction, there are a number of reports that indicate that these cells also receive signals from cone/rod pathways (Belenky et al. 2003; Dacey et al. 2005; Perez-Leon et al. 2006; Wong et al. 2007). Perez-Leon et al. (2006), using retrograde labeling from the SCN of rats and whole cell recordings, reported that approximately 5% of ipRGCs demonstrate light-evoked synaptic inputs, whereas Wong et al. 2007 reported, using multielectrode array recordings in rat retina, that all ipRGCs receive synaptic input from the outer retina. Furthermore, Lupi et al. 2006 demonstrated light-evoked c-Fos induction in the SCN of melanopsin knockout mice as early as P14, indicating rod/cone signaling to the SCN. However, it is unclear whether the rod/cone-mediated signals reaching the SCN at P14 are a result of the formation synaptic inputs onto ipRGCs or the result of inputs from other types of ganglion cells to the SCN. Additionally, because previous assessments of early postnatal ipRGC light responses have been performed in the presence of synaptic blockers (Sekaran et al. 2005; Tu et al. 2005), it is still unclear at what point in development ipRGCs begin to show synaptically driven light responses and what the functional impact of those synaptic connections might be. Because of the differences between the image-forming and nonimage-forming streams in the visual system, it is possible that these two visual systems do not develop coincidentally (Sernagor 2005).

The goal of this study was to record light responses of ipRGCs throughout development and to determine the timing and functional impact of the formation of extrinsic inputs onto these cells. We investigated the properties of developing ipRGCs during the first postnatal weeks using a novel transgenic mouse model in which ipRGCs are labeled in vivo with enhanced green fluorescent protein (EGFP). We found that ipRGC light responses during this period transition from being

Address for reprint requests and other correspondence: P. Kofuji, Department of Neuroscience, University of Minnesota, 6-145 Jackson Hall, 321 Church St. SE, Minneapolis, MN 55455 (E-mail: kofuj001@umn.edu).

The costs of publication of this article were defrayed in part by the payment of page charges. The article must therefore be hereby marked "*advertisement*" in accordance with 18 U.S.C. Section 1734 solely to indicate this fact.

driven solely by "intrinsic" phototransduction to being driven by both "intrinsic" and "extrinsic" phototransduction right around the time of eye opening. Emergence of cone/rod modulation of ipRGCs is coincident with the stratification of their dendrites in the inner plexiform layer (IPL), mainly in the ON sublamina. Overall, these results indicate that ipRGCs undergo major changes in their light sensitivity and synaptic connectivity during a crucial period in visual development.

METHODS

Generation of Opn4-EGFP bacterial artificial chromosome (BAC) transgenic mouse line

BAC recombination was performed by using protocols and reagents from a BAC Modification Kit (Gene Bridges, Heidelberg, Germany), which relies on an ET-recombination method (Muyrers et al. 1999). The BAC clone RP24-107C11, containing approximately 29 and 155 kb of DNA flanking the 5′ and 3′ ends of the *Opn4* gene locus, respectively, was obtained from the BAC resource at Children's Hospital Oakland Research Institute, and a cassette containing an EGFP-PolyA (Clontech, Mountain View, CA) and a kanamycin/neomycin resistance gene flanked by two FLP recombinase target (FRT) sites was inserted. Briefly, we used polymerase chain reaction (PCR) to amplify the *Opn4* gene homology arms and the EGFP-FRT-kanamycin/neomycin-FRT cassette. *Opn4* gene arm 1 consisted of a 50-bp fragment upstream of the ATG in exon 1 (5′-GGA CCG ATC CCT GAT CTT TCC ATG GCC TTA GCT CCT CTG AGA GCC TGA GC-3′). *Opn4* gene arm 2 was a 50-bp product downstream of the stop codon of exon 9 (5′-CAC AGT CAC ATG CAG ATA TTC CCC TAG ATA CAG ATC ATA CTT AGA CCC TG-3′). The EGFP-FRT-kanamycin/neomycin-FRT cassette was derived from the pIGCN21 plasmid (kindly provided by N. Copeland and N. Jenkins, National Cancer Institute) in which we replaced the *EGFP-cre* gene with EGFP-polyA. *Escherichia coli* cells carrying RP24-107C11 BAC and the plasmid pRedET were electroporated with the Opn4 (arm 1)-EGFP-FRT-Neo/Kan-FRT-Opn4 (arm 2) PCR product, and homologously recombined positive clones were selected with kanamycin and chloramphenicol. The kanamycin/neomycin cassette was then removed by electroporating the plasmid containing flp recombinase (plasmid 706-FLP, GeneBridges, Heidelberg, Germany), resulting in an Opn4-EGFP BAC. Homologous recombination was confirmed by PCR and by sequencing the BAC using primers that flanked the upstream of Opn4 arm 1 to EGFP cassette and downstream of Opn4 arm 2 to the EGFP cassette. The Opn4-EGFP BAC DNA was prepared using a modified alkaline lysis protocol (Nucleobond kit, Clontech) and circular intact DNA was microinjected into fertilized embryos (FVB/NCR strain) by standard pronuclear injection techniques at the McLaughlin Research Institute (Great Falls, MT). Genomic DNA isolated from tissue was purified using a Puragene kit (Gentra Systems, Minneapolis, MN) and founder mice carrying the BAC transgene were identified by PCR with primer sets 5′-GAC ATT AAG CAG TCA GCA GC-3′ (in *Opn4* gene) and 5′-GTG GTG CAG ATG AAC TTC AG-3′ (in EGFP), yielding an approximately 380-bp product. One founder line was produced that transmitted the transgene in a normal Mendelian inheritance pattern with all offspring appearing grossly normal. Animals were cared for in accordance with guidelines described in the *Guide for the Care and Use of Laboratory Animals*, using protocols approved by the University of Minnesota Institutional Animal Care and Use Committee.

Antibodies

The following primary antibodies were used: rabbit anti-melanopsin (obtained from I. Provencio, UF006, University of Virginia), rabbit anti-EGFP (Invitrogen, Carlsbad, CA), mouse anti-EGFP (Invitrogen), and goat anti-choline acetyl transferase (ChAT; Millipore, Bedford, MA). For secondary antibodies, we used AlexaFluor antibodies (Invitrogen) produced in goat or donkey, including anti-rabbit 488 and 594; anti-mouse 488 and 594; and anti-goat 488 and 594.

Immunocytochemistry

Mice were killed with CO_2 asphyxiation and were intracardially perfused with 4% paraformaldehyde/0.1 M phosphate buffer (PFA). Retinas were dissected in phosphate-buffered saline (PBS), pH 7.4, and were fixed overnight in PFA at 4°C. The next day, retinas were washed extensively in PBS, then blocked overnight in PBS containing 10% goat or donkey serum and 0.5% Triton X-100 at room temperature. Primary antibody incubation was carried out for 3 days at 4°C in PBS containing 1% goat or donkey serum and 0.5% Triton X-100. Samples were washed three times for 15 min each in PBS and then incubated in secondary antibodies for 2 days at 4°C. Retinas were washed three times for 15 min in PBS and then mounted in Vectashield (Vector Laboratories, Burlingame, CA). When the experiment was carried out using a pipette solution containing 0.5% biocytin (Sigma, St. Louis, MO) or neurobiotin (Vector Laboratories), patch pipettes were carefully detached from the recorded cells and the retinas were then fixed with PFA overnight at 4°C. Neurobiotin or biocytin was visualized with rhodamine-conjugated streptavidin (Jackson ImmunoResearch Laboratories, West Grove, PA).

Image analysis

The fluorescent specimens were imaged with a Olympus Fluoview 1000 confocal microscope, using a ×40 or ×60 oil-immersion lens. Excitation at different wavelengths was performed sequentially to prevent bleed-through of images. Optical sections were collected at 0.2- to 1.0-μm intervals and reconstructions of several optical images onto a single plane were performed using National Institutes of Health ImageJ software (http://rsb.info.nih.gov/ij/). The brightness and contrast of the images were adjusted using ImageJ software. For analysis of dendritic stratification in the IPL, we used ChAT immunostaining to reveal bands corresponding to the projections of cholinergic amacrine cells. These bands were used as reference landmarks for sublamina a (OFF sublamina) and b (ON sublamina) and were used to categorize ipRGC dendritic arborization. For dendritic analysis, three-dimensional reconstructions of the dendritic processes of each biocytin/neurobiotin-filled neuron were made from Z-series stacks of confocal images. The projection images were semiautomatically traced with ImageJ using the NeuronJ plugin (http://www.imagescience.org/meijering/software/neuronj/). Total dendritic length and dendritic field size of each filled cell were analyzed. Dendritic field area was calculated by drawing a convex polygon linking the dendritic terminals. The dendritic field area was then calculated and the diameter expressed as that of a circle having an equal area.

Electrophysiology

Whole cell recordings were performed on acutely isolated whole-mount retinas of Opn4-EGFP mice. Animals were anesthetized with isoflurane and then killed by pneumothorax after which the eyes were enucleated. Retinas were removed from eyecups and placed in Ames' solution containing 23 mM sodium bicarbonate bubbled in 95% O_2-5% CO_2 at room temperature. Prior to recording, the vitreous was removed and retinas were treated with Ames' solution (Sigma) containing collagenase/hyaluronidase (240 and 1,000 U/ml, respectively) at room temperature for 20 min. For animals younger than P11 the collagenase/hyaluronidase treatment was shortened to 5 min. Retinas were then mounted with the vitreal surface up in a custom-made chamber (Newman and Bartosch 1999) and perfused with Ames' solution bubbled with 95% O_2-5% CO_2 at room temperature. Euthanasia and dissections were performed in ambient room light. Dissec-

tions were performed under a standard dissection microscope that was also used to mount retinas in the recording chamber. At all other times following dissection, retinas were kept in a dark room with only minimal ambient light. The recording chamber was mounted on the stage of an upright microscope (E600 FN, Nikon, Tokyo, Japan) equipped with differential interference contrast optics and epifluorescence. Recordings were performed at room temperature (21–23°C) using an Axopatch 200B amplifier (Axon Instruments/Molecular Devices, Sunnyvale, CA) with fire-polished borosilicate pipettes (3–7 mΩ; Sutter Instruments, Novato, CA) filled with (in mM) 125 K-gluconate, 2 $CaCl_2$, 2 $MgCl_2$, 10 EGTA, 10 HEPES, 0.5 NaGTP, and 2 Na_2ATP, pH with KOH (pH 7.2). All traces were sampled at 5–10 kHz and low-pass filtered at 2–5 kHz. Current and voltage acquisitions were performed with a Digidata 1322 D/A and A/D converter connected to a personal computer running pCLAMP 10 software (Axon Instruments). Liquid junction potentials (6.1 mV) were corrected for all recordings. In full-field white-light experiments, cells were given 3–5 min following visualization of GFP under fluorescence prior to stimulation with white light. In these experiments, each cell was stimulated only once after patching. In irradiance–response experiments, retinas were allowed to dark adapt for 5 min before the first stimulus and light stimuli following the first stimulus were spaced 3 min apart to allow the cell to return to baseline.

Whole cell currents were analyzed off-line with Clampfit (Axon Instruments) and membrane potential values were averaged over 1-s sliding time windows with IgorPro 6.0 (Portland, OR). Baseline resting membrane potential (V_m) was measured by taking the average membrane voltage over 10 s of baseline prior to light stimulation. Measurements of cell capacitance (C_m) and resistance (R_m) were derived from those currents evoked by stepping the cell potential to a 10-mV hyperpolarized value for 20 ms from a holding potential of −60 mV. Only cells with an access resistance of <20 MΩ were used for these calculations. Charge Q was estimated by time integration of evoked current during the step voltage. Membrane resistance was estimated from the steady-state–evoked current during the step voltage. Light responses were defined as the maximum depolarization of the averaged trace during or following light stimulation within a 50-s time window. ON latency was defined as the time to reach 50% of the maximum response after light on (latency to half-maximum). OFF latency was defined as the time of decay to 50% of the maximum light response at or following light off. Because of extensive averaging of traces prior to analysis, times of light on and off were defined based on the beginning of the ON and OFF components of an averaged response from a reference trace and then extrapolated to other traces. Curve fits for normalized, averaged irradiance–response data were determined by nonlinear regression using Origin 7.5 (MicroCal, Northampton, MA) according to the logistic dose–response function: $y = A_2 + [(A_1 - A_2)/1 + (IR/IR_{50})^{nH}]$, where A_1 is the maximum response plateau, A_2 is the minimum response plateau, IR is irradiance, IR_{50} is the irradiance values that generate half-maximal response, and n_H is the Hill slope. Light stimuli for some experiments were full-field, broadband white light (7.6×10^{14} photons·cm^{-2}·s^{-1} at 480 nm) delivered from below the retina using the microscope's 100-W halogen lamp and transillumination optics. An electromechanical shutter (Vincent Associates, Rochester, NY) was used to control the duration and timing of the light stimulus. In irradiance–response experiments, light stimulation was performed using a xenon lamp feeding the camera port. A filter wheel fitted with various neutral-density filters and narrow band-pass filters (Chroma Technologies, Rockingham, VT) and shutter (Lambda-3, Sutter Instruments) was used to control the wavelength, intensity, and duration of light stimuli. Irradiance measurements were made with a calibrated radiometer model S370 (UDT Instruments, San Diego, CA).

Pharmacology

To block transmission of signals from the outer retina to ipRGCs, we blocked bipolar cell light responses with a cocktail consisting of 250 μM DL-2-amino-4-phosphonobutyrate (DL-AP4, a group III metabotropic glutamate receptor agonist); 10 μM 6,7-dinitroquinoxaline-2,3-dione (DNQX) or 75 μM 6-cyano-7-nitroquinoxaline-2,3-dione (CNQX) [both α-amino-3-hydroxy-5-methyl-4-isoxazolepropionic acid (AMPA)/kainate receptor antagonists]. D-AP4, CNQX, and DNQX were purchased from Tocris (Ellisville, MO). To block gap junctions, we used the gap-junction blocker meclofenamic acid (MFA; Sigma) at a working concentration of 200 μM. The retinas were preincubated with MFA for 20 min prior to recordings.

Statistics

Statistical analyses were performed using Origin 7.5 (MicroCal). Statistical comparison of means was made using either a Student's *t*-test or one-way ANOVA, and significance was concluded when $P < 0.05$. Post hoc analyses were done using Tukey's honestly significant difference. Data are presented as means ± SE.

RESULTS

Generation and validation of Opn4-EGFP BAC transgenic mice

Visualization of ipRGCs in newborn and early postnatal mouse retinas is difficult given the need for injection of retrograde tracers into SCN or other brain areas innervated by these cells (e.g., Berson et al. 2002; Dacey et al. 2005; Lucas et al. 2003). Therefore to study the functional and morphological properties of ipRGCs during early postnatal development, we have taken a BAC transgenic approach to allow for the in vivo labeling of ipRGCs in the mouse retina with EGFP. For generation of this transgenic mouse line, we used a BAC containing the *Opn4* gene and 29 kb of the 5′ and 155 kb of the 3′ sequences (Fig. 1*A*). In this BAC, the coding sequence for *Opn4*, which is contained in multiple exons, was replaced with EGFP and polyadenylation sequences by in vitro recombination (Yang et al. 1997). From this recombinant BAC, a single founder mouse line was generated. Adult and young animals from the Opn4-EGFP line appeared behaviorally normal, with no gross abnormalities in motor activity. We detected intrinsic EGFP fluorescence only in the retina (Fig. 1*B*), with no detectable fluorescence found in paraformaldehyde-fixed samples of brain tissue (data not shown). RT-PCR analysis of EGFP expression also confirmed the restricted expression of EGFP to the retina (Supplemental Figs. S1 and S2).[1] EGFP fluorescence in the ganglion cell layer was easily visible through the microscope under epifluorescent illumination. Cells of varying intensity could be readily identified, with some cells showing a very strong EGFP signal and others, although still visible, showing weaker fluorescent labeling.

To validate this mouse line as a reporter of melanopsin expression, it was essential to demonstrate that there was a correlation of expression between the reporter gene EGFP and endogenous melanopsin in RGCs. By using anti-melanopsin and anti-EGFP antibodies in whole-mount retinas from Opn4-EGFP mice, we were able to verify that EGFP expression colocalized with melanopsin expression in RGCs (Fig. 1*C*). Whereas EGFP expression was localized to the cytosol of the

[1] The online version of this article contains supplemental data.

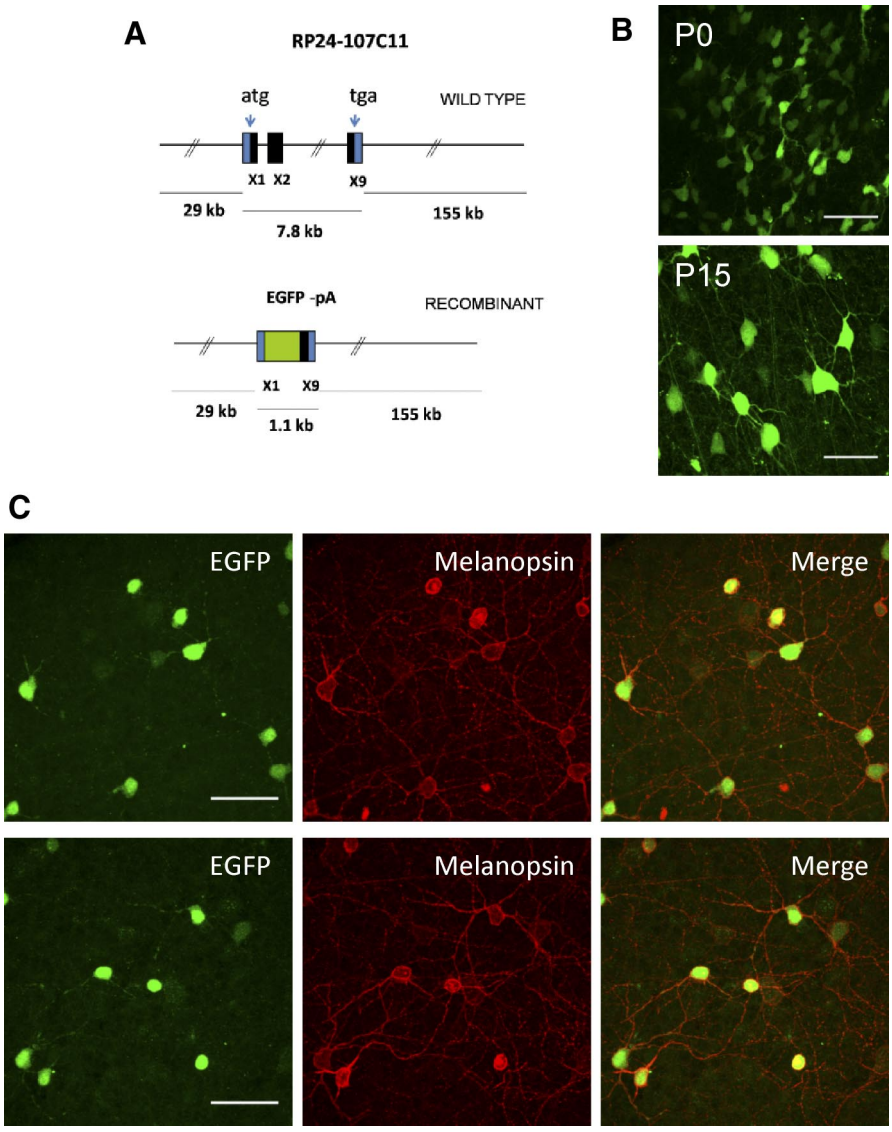

FIG. 1. Generation and initial characterization of Opn4-enhanced green fluorescent protein (EGFP) mouse line. *A*: schematic representation of the transgene Opn4-EGFP. The 192-kb mouse genomic bacterial artificial chromosome (BAC) clone RP24-107C11 containing the entire transcriptional unit of Opn4 together with 29 kb of upstream and 155 kb of downstream sequence was engineered to harbor EGFP coding sequences followed by a polyadenylation (pA) signal in the coding region of the *Opn4* gene by homologous recombination in *Escherichia coli*. X1, X2, and X9 represent exon 1, exon 2, and exon 9 with the start codon in exon 1 (ATG) and stop codon (TGA) in exon 9. *B*: confocal images of intrinsic EGFP signals in whole-mount retinas of Opn4-EGFP mouse at postnatal day 0 (P0, *top*) and P15 (*bottom*). *C*: immunostaining for EGFP (green) and melanopsin (red) of adult (P21) whole-mount EGFP-Opn4 retinas. Scale bar: 50 μm (*B* and *C*).

soma and dendrites, as would be expected for expression of cytoplasmic EGFP (Fig. 1*C*, *left panels*), the expression of melanopsin was restricted to the plasma membrane of RGC somas and processes (Fig. 1*C*, *middle panels*). Of cells that were EGFP-positive, 95.6% (306/320 EGFP-positive cells) in P17–P24 retinas and 99.0% (417/421 EGFP-positive cells) in P5–P7 retinas also stained positive for melanopsin. Of cells that stained positive for melanopsin 97.8% (306/313 melanopsin-positive cells) in P17–P24 retinas and 99.8% (417/418 melanopsin-positive cells) in P5–P7 retinas also stained positive for EGFP (Fig. 1*C* and data not shown). The strong coexpression of EGFP and melanopsin demonstrates that EGFP is indeed being expressed with high coincidence in RGCs that express melanopsin.

We next wanted to functionally validate that EGFP-positive cells in this reporter mouse are intrinsically photosensitive, as would be expected if EGFP is indeed being expressed in ipRGCs. To test this, we performed whole cell recordings of light responses of EGFP-positive cells at a variety of ages from early postnatal (P0–P2 and P5–P7) to early adult (P17–P24). Intrinsic EGFP fluorescence in the retinas of these mice was detectable at P0. EGFP-positive cells were also visible in the inner nuclear layer (INL) at P17–P24 and EGFP expression in these cells colocalized with melanopsin expression (data not shown). This is consistent with previous research showing that some melanopsin-positive cell bodies are found in the INL (Berson et al. 2002; Dacey et al. 2005; Hattar et al. 2002). Recordings were performed in a whole-mount retinal preparation that preserves light responsiveness of retinal cells (Metea and Newman 2006), presumably arising from the remaining retinal pigmented epithelial cells in this preparation. To identify ganglion cells, retinas were visualized under infrared illumination and then EGFP-positive cells in the ganglion cell layer (GCL) were localized by brief exposure to 480-nm illumination. To determine intrinsic photosensitivity of EGFP-positive cells, we performed recordings in the presence of an AMPA/kainate (DNQX/CNQX) glutamate receptor antagonist and a metabotropic (DL-AP4) glutamate receptor agonist to block signaling to RGCs from the outer retina via the ON and OFF bipolar cell pathways. EGFP-positive cells at every age tested showed an increase in firing rate following a 5-s full-field white-light stimulus (Fig. 2). Smoothing of voltage responses reveals the characteristic slow, tonic depolarization first reported by Berson et al. 2002 (ON latency: P0–P2: 4.5 ±

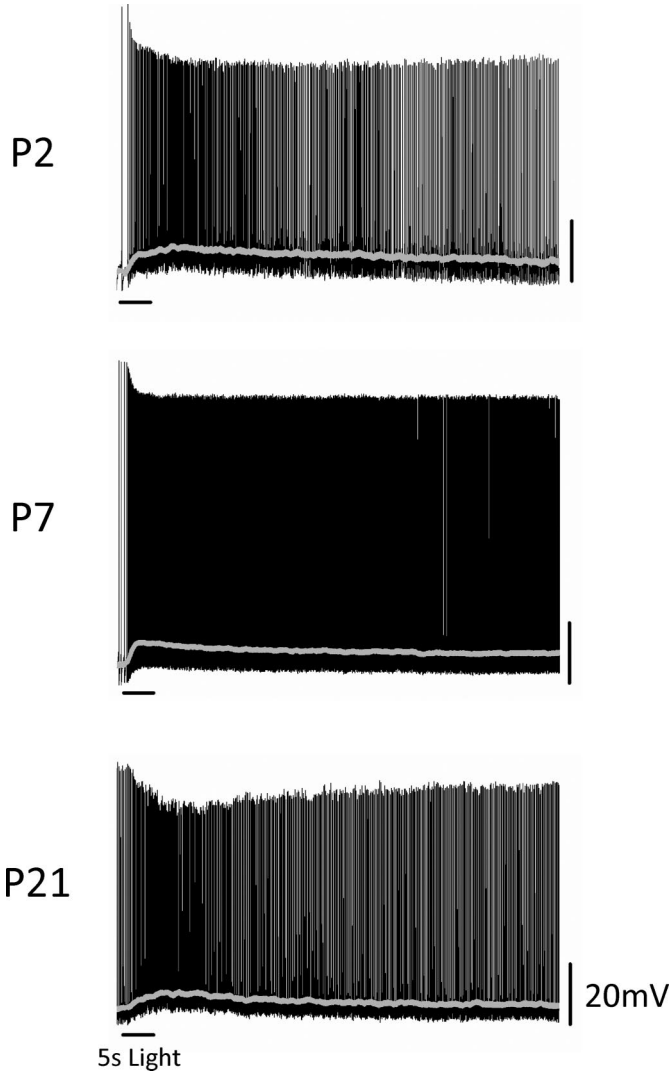

FIG. 2. Intrinsic light responses of EGFP-positive ganglion cells in whole-mount Opn4-EGFP retinas. Membrane potential of EGFP-positive ganglion cells was recorded in current-clamp mode at ages P2, P7, and P21. A full-field white-light stimulus of 5-s duration was applied to the retina. A cocktail of pharmacological blockers was also included to prevent any rod- or cone-driven influences in the light responses. Gray line shows membrane potential values averaged over a 1-s sliding time window.

0.8 s, $n = 14$; P5–P7: 2.0 ± 0.1 s, $n = 5$; P17–P24: 2.7 ± 0.7 s, $n = 10$). The ipRGC response declined to baseline levels only after several seconds following termination of the light stimulus (OFF latency: P0–P2: 22.8 ± 2.3 s, $n = 14$; P5–P7: 52.0 ± 11.4 s, $n = 5$; P17–P24: 16.3 ± 3.0 s, $n = 10$). At P17–P24, the average peak depolarization amounted to 6.8 ± 0.8 mV ($n = 10$), which is similar to the average peak depolarizations of 5.9 ± 0.8 mV ($n = 14$) and 7.2 ± 1.0 mV ($n = 5$) at early postnatal stages (P0–P2 and P5–P7, respectively) ($P > 0.75$, one-way ANOVA). Overall, the kinetics of light responses obtained from EGFP-positive cells in the presence of synaptic blockers are consistent with those reported for rat and mouse ipRGCs (Berson et al. 2002; Hattar et al. 2002; Warren et al. 2006) and demonstrate that EGFP-positive cells in this reporter mouse line are indeed intrinsically photosensitive.

Of note, in the presence of synaptic blockers it was common to see prestimulus spontaneous firing at P0–P2, P5–P7, and P17–P24. In the absence of synaptic blockers, it was more common to see prestimulus spontaneous firing prior to light stimulation in cells at P17–P24 compared with P0–P14, which is likely indicative of the partially light adapted state of the retinas. However, there were also cells at every age (including P17–P24) for which we observed no background firing, consistent with previous studies demonstrating very low levels of spontaneous activity for these cells in the absence of light stimulation (data not shown) (Berson et al. 2002; Warren et al. 2003).

ipRGCs change how they respond to light throughout development

Previously, calcium imaging and multielectrode array techniques were used to analyze the responsiveness of ipRGCs to light at early developmental stages (Sekaran et al. 2005; Tu et al. 2005). These reports made use of various synaptic blockers or knockout mice to isolate adult cells with intrinsic light sensitivity and compare them to early postnatal cells. With the genetic labeling of ipRGCs, it was our goal to compare the functional properties of ipRGCs during the first three postnatal weeks of development in the absence of synaptic blockers. We compared the light responses of ipRGCs to a 5-s full-field white-light stimulus at four different developmental periods during the first three postnatal weeks of development: just after birth (P0–P2), before eye opening (P5–P7), around the time of eye opening (P11–P14), and early adulthood (P17–P24) (Sernagor et al. 2001). The ability to perform whole cell recordings of cells at these various ages allowed us to measure resting membrane potential (V_m), capacitance of the membrane (C_m), and resistance of the membrane (R_m) of cells throughout development (Table 1). The higher capacitance of cells at P5–P7 and P11–P14 than that of those at P0–P2 or P17–P24 would support the idea that ipRGCs are gap-junctionally coupled during these stages. As a preliminary test of

TABLE 1. *Intrinsic electrical properties of ipRGCs recorded at various stages of postnatal development in the absence or presence of MFA*

		C_m, pF		R_m, MΩ	
Age Group	V_m, mV	Control	MFA	Control	MFA
P0–P2	−52.9 ± 1.9 ($n = 8$)	32.8 ± 1.7 ($n = 13$)	33.9 ± 2.0 ($n = 7$)	868.7 ± 51.8 ($n = 13$)	607.9 ± 103.5* ($n = 7$)
P5–P7	−57.0 ± 1.3 ($n = 25$)	55.5 ± 1.6 ($n = 17$)	48.7 ± 1.6*† ($n = 18$)	403.9 ± 50.1 ($n = 17$)	432.4 ± 55.3 ($n = 20$)
P11–P14	−55.0 ± 0.9 ($n = 39$)	58.5 ± 1.7 ($n = 19$)	38.8 ± 2.6* ($n = 21$)	414.4 ± 46.5 ($n = 19$)	369.9 ± 25.2 ($n = 21$)
P17–P24	−50.5 ± 1.0 ($n = 19$)	41.6 ± 1.7 ($n = 20$)	31.6 ± 2.3* ($n = 15$)	370.2 ± 36.1 ($n = 20$)	515.9 ± 36.5* ($n = 15$)

Values are means ± SE. V_m, resting membrane potential; C_m, membrane capacitance; R_m, membrane resistance; MFA, meclofenamic acid. *Indicates significant difference from control condition ($P < 0.05$). †Two outliers (>2SDs from the mean) were removed from the analysis.

this hypothesis, we measured the capacitance and resistance of cells at each of these four stages in the presence of 200 μM MFA, a potent antagonist of several types of neuronal gap junctions in the retina (Pan et al. 2007). We expected that if cells were coupled at these stages, the presence of MFA would decrease the average C_m. Indeed, we found that in the presence of MFA the C_m was significantly lower in cells at P5–P7 ($P < 0.005$, Student's t-test), P11–P14 ($P < 0.0001$, Student's t-test), and, interestingly, also at P17–P24 ($P < 0.002$, Student's t-test), but not at P0–P2 ($P > 0.6$, Student's t-test) (Table 1). This is consistent with the idea that ipRGCs are gap-junctionally coupled as early as P5 in the developing mouse retina and continue to be electrically coupled with other retinal cells into early adulthood (Sekaran et al. 2003, 2005; Tu et al. 2005). The results concerning R_m, however, are less clear. If R_m at any of these stages is influenced by gap-junctional coupling, we would expect the presence of MFA to increase R_m. At P17–P24, cells in MFA did have a significantly higher R_m than did cells in the control condition ($P < 0.009$, Student's t-test), but at P0–P2 cells in MFA had a significantly lower R_m than did cells in the control condition. There was no effect of MFA on the R_m of cells at P5–P7 ($P > 0.07$, Student's t-test) or P11–P14 ($P > 0.3$, Student's t-test). It is unclear why these differential effects of MFA on R_m occurred at different ages, but previous research has shown that MFA can affect other channel types (especially potassium channels) within neurons in addition to gap junctions, which could affect the R_m of the cells (Lee and Wang 1999; Peretz et al. 2005).

Examples of light responses seen during each period are shown in Fig. 3*A*. At P0–P2 and P5–P7, all of the cells responded to light with the characteristic long latency and sustained depolarization characteristic of melanopsin-mediated responses. Additionally, at early stages (P0–P7), periodic bursts of action potentials independent of light stimulation were observed in 79% of cells (62/78) in accordance with previous studies (Wong 1999) (Supplemental Fig. S3). The average peak light-evoked depolarization increased during development with significantly larger responses at P17–P24 (18.6 ± 1.2 mV, $n = 21$) than at P0–P2 (7.7 ± 1.9 mV, $n = 8$), P5–P7 (9.7 ± 1.1 mV, $n = 25$), or P11–P14 (14.5 ± 0.8 mV, $n = 39$) ($P < 0.001$, one-way ANOVA) (Fig. 3*B*). Interestingly, between P11 and P14, some of the cells (15/39) displayed a rapid onset response of short latency. This initial fast component was always excitatory and cells remained depolarized for the duration of the light stimulus. Following light off, cells displayed a rapid repolarization of short latency. Spike frequency remained elevated even after the decay time criterion was met, consistent with a residual melanopsin-mediated response. These rapid onset and offset kinetics were observed in most (17/21 for full-field white light and 22/26 for 610- or 480-nm light, total of 39/47) cells at P17–P24. One-way ANOVAs revealed that the ON and OFF latencies of cells at P17–P24 were indeed significantly faster than cells at P0–P2 and P5–P7 (ON latency: $P < 0.001$, one-way ANOVA; OFF latency: $P < 0.001$, one-way ANOVA) (Fig. 3, *C* and *D*). Because traces were averaged over a 1-s sliding time window

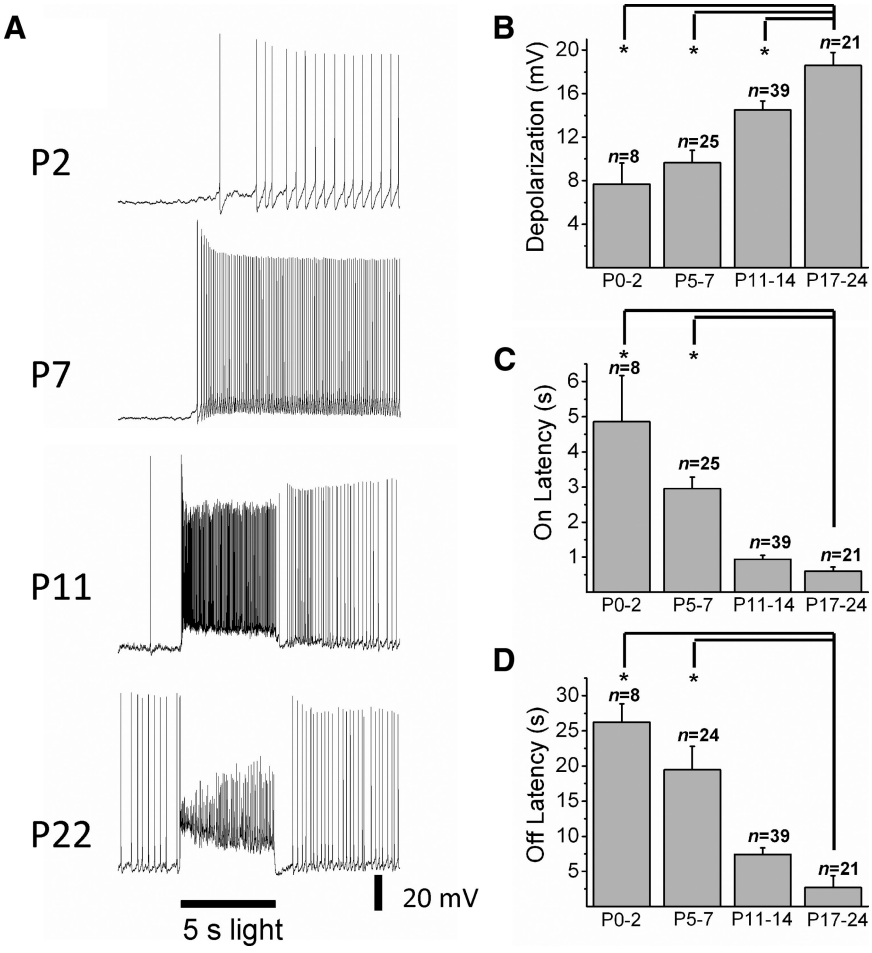

FIG. 3. Light-evoked responses of intrinsically photosensitive retinal ganglion cells (ipRGCs) at various stages of mouse development. *A*: recordings of representative light responses at P2, P7, P11, and P22 in response to a 5-s full-field white-light stimulus in the absence of synaptic blockers. Amplitude (mean ± SE) of average depolarization (*B*) ON latency (*C*) and OFF latency (*D*) are shown for the various stages of mouse development (ON latency: P0–P2 = 4.9 ± 1.3 s; P5–P7 = 3.0 ± 0.3 s; P11–P14 = 0.9 ± 0.1 s; P17–P24 = 0.6 ± 0.1 s and OFF latency: P0–P2 = 26.2 ± 2.6 s; P5–P7 = 19.5 ± 3.4 s; P11–P14 = 7.4 ± 0.9 s; P17–P24 = 2.7 ± 1.7 s). Error bars represent SE. *$P < 0.001$.

prior to analysis of ON and OFF latencies, it is likely that the kinetics of the light responses are somewhat distorted. ON and OFF latencies for cells receiving extrinsic inputs are much faster than those measured from averaged traces, with both being on the order of <200 ms when measured from the raw traces (data not shown). However, without averaging, measurements of membrane voltages are difficult to perform objectively on spiking cells, especially in younger animals where the slower intrinsic response dominates. Therefore to compare kinetics across ages, we chose to quantify and compare these values using smoothed traces.

The differential kinetics of light responses seen in early adult ipRGCs would be consistent with these cells receiving cone/rod-mediated signals from the outer retina, as was recently demonstrated by studies in primate and rat retina (Dacey et al. 2005; Wong et al. 2007). To test this, we recorded light responses of cells to full-field white-light stimuli at P17–P24 before and after application of synaptic blockers (DL-AP4 and DNQX/CNQX) to block cone/rod-mediated ON and OFF pathways (Fig. 4, *A–C*). Indeed, in the presence of a cocktail of synaptic blockers, the ON and OFF latencies for light-evoked depolarizations were significantly increased compared with controls (ON latency: 0.6 ± 0.02 vs. 2.7 ± 0.7 s, $n = 10$; $P < 0.01$, Student's *t*-test; OFF latency: 0.4 ± 0.1 vs. 16.3 ± 3.0 s, $n = 10$; $P < 0.001$, Student's *t*-test) (Fig. 4, *E* and *F*). Additionally, maximum depolarization significantly decreased

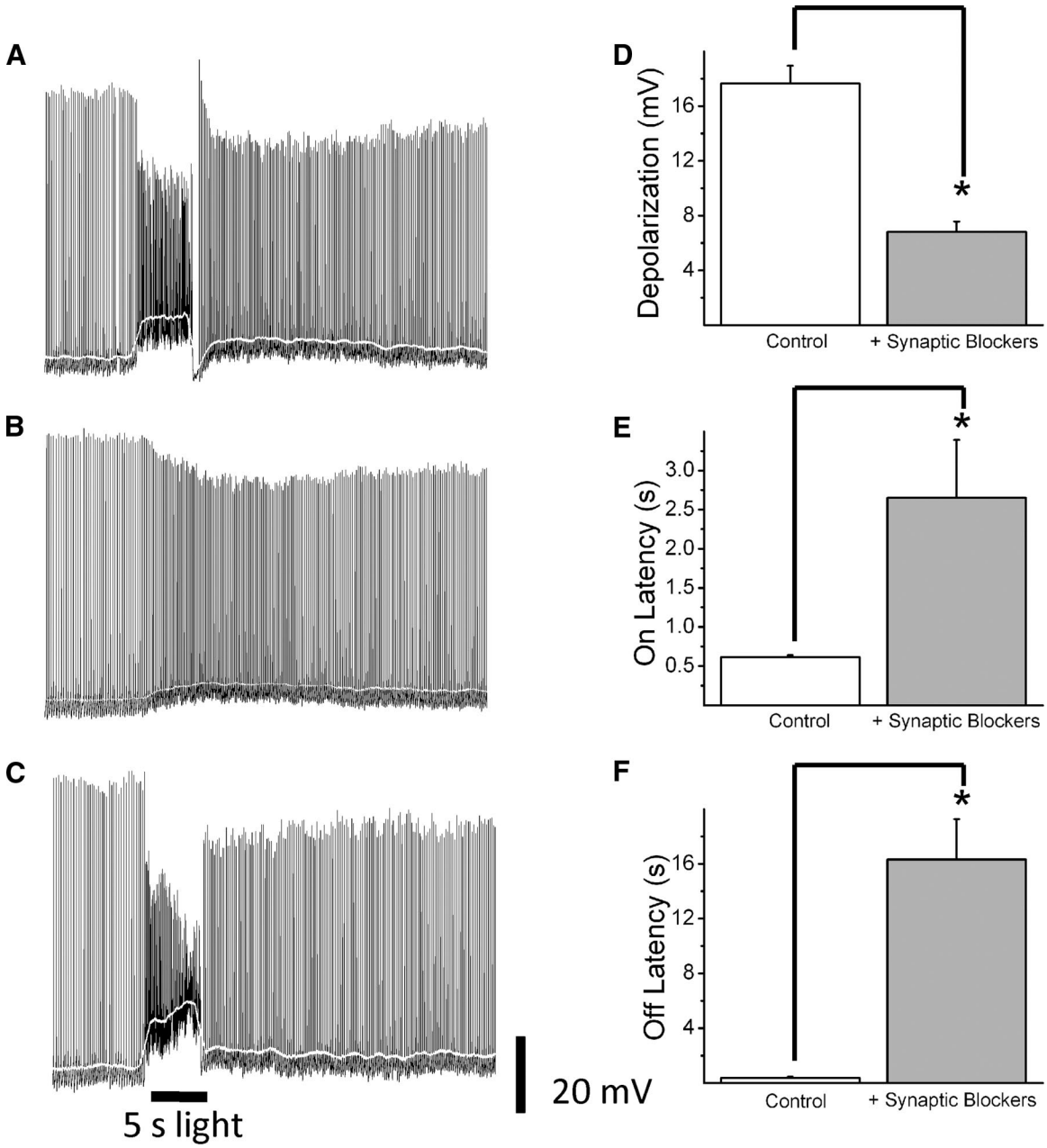

FIG. 4. Influence of glutamatergic synaptic inputs on ipRGC light-evoked responses. Representative traces of an ipRGC response to a 5-s full-field white-light stimulus from a P21 mouse recorded in the absence (*A*) or presence (*B*) of a cocktail of glutamatergic receptor blockers. Traces in *C* show the same cell on washout of the synaptic blockers. Amplitude (mean ± SE, $n = 10$) of depolarization (*D*) ON latency (*E*) and OFF latency (*F*) are shown in the absence and presence of synaptic blockers. White line shows membrane potential values averaged over a 1-s sliding time window. Error bars represent SE. *$P < 0.01$.

after synaptic blockade (17.7 ± 1.3 vs. 6.8 ± 0.8 mV, $n = 10$; $P < 0.0001$, Student's *t*-test) (Fig. 4*D*). Because these extrinsic inputs are causing ipRGCs to respond to light with a larger depolarization than the intrinsic response alone, the increased proportion of cells during development displaying these extrinsically driven responses (0% at P5–P7, 38.5% at P11–P14, and 83% at P17–P24) is most likely responsible for the increase in light-evoked depolarization seen during development (see Fig. 3*B*) rather than a change in the properties of the extrinsic response. If depolarization of extrinsically responding cells to a 5-s white-light stimulus is compared between P11–P14 and P17–P24, there is no difference in the mean light-evoked depolarization (P11–P14: 18.3 ± 1.2 mV, $n = 15$; P17–P24: 17.2 ± 1.4 mV, $n = 14$; $P = 0.56$, Student's *t*-test). From these observations it is reasonable to conclude that the two types of kinetics observed in ipRGC light responses are the result of two different systems: *1*) the intrinsic response, mediated by melanopsin and insensitive to synaptic blockers; and *2*) the extrinsic response, mediated by cone/rod-driven pathways and sensitive to synaptic blockers.

Responses of ipRGCs to various levels of irradiance during development

We expected that the outer retinal signals from rods/cones present by P17–P24 might serve to increase the sensitivity of adult cells to light in comparison to ipRGCs at P5–P7, which rely solely on intrinsic signals for light responsiveness (Dacey et al. 2005; Wong et al. 2007). To test this, we compared the light responsiveness of ipRGCs at various developmental periods (P0–P2, P5–P7, and P17–P24) to increasing intensities of 5-s 480- or 610-nm light stimuli. As expected, ipRGCs responded to increasing irradiance with stronger depolarizations of shorter latency, eventually saturating. Examples of light responses for each age period to increasing intensities of 480-nm light stimuli are shown in Fig. 5. When ipRGC responses to increasing irradiance levels were normalized and then averaged for groups P5–P7 and P17–P24 and plotted according to light intensity, there was an indication that adult cells are more sensitive to 480-nm light stimulation than P5–P7 cells by approximately one log unit of irradiance (Fig. 6*A*), a trend that was also evident for 610-nm light stimulation (Fig. 6*B*). The light responses at P5–P7 lie in the photopic range (Dacey et al., 2005), consistent with previous results indicating low levels of light sensitivity for melanopsin (Sekaran et al. 2005; Tu et al. 2005).

If the higher sensitivity at P17–P24 is generated by synaptic signals originating from the outer retina, then these differences should vanish in the presence of synaptic blockers. To test this, we performed additional irradiance–response experiments as described earlier, but in the presence of a synaptic blocker cocktail (DNQX and DL-AP4). Irradiance–response curves of cell responses in the presence of synaptic blockers for P5–P7 and P17–P24 are shown in Fig. 6, *C* and *D*. In the presence of synaptic blockers, the higher sensitivity of cells at P17–P24 to both 480- and 610-nm light was diminished. This indicates that the increased sensitivity of P17–P24 ipRGCs is due to the presence of functional extrinsic inputs at this age and not to an enhancement of sensitivity in the intrinsic system between P5–P7 and P17–P24.

Because ipRGCs are receiving functional synaptic inputs at P17–P24, but not at P5–P7, it would be reasonable to expect that the spectral sensitivity of ipRGCs at P17–P24 would be shifted toward a λ_{max} more consistent with midwavelength cone-driven input, which has a λ_{max} of about 510 nm. How-

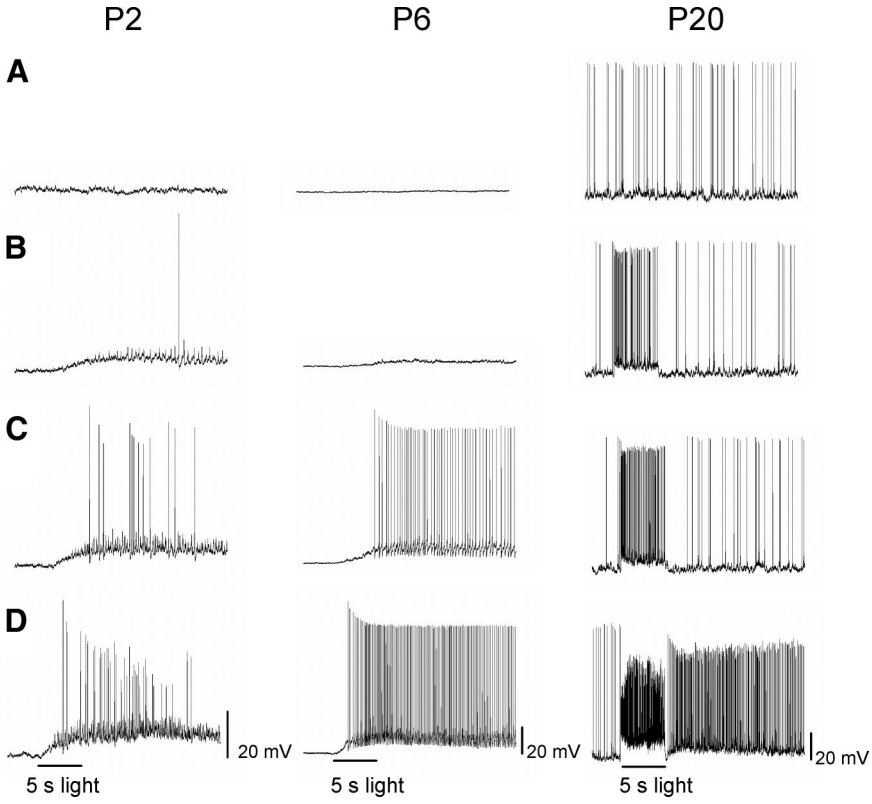

FIG. 5. Light-evoked responses of ipRGCs to increasing (*top* to *bottom*) intensities of 5-s full-field 480-nm light stimulation. Representative light responses at P2 (*left column*), P6 (*middle column*), and P20 (*right column*). Stimulus intensity (in photons·cm^{-2}·s^{-1}) for P2: 2.28×10^9 (*A*), 2.28×10^{10} (*B*), 6.84×10^{10} (*C*), and 2.28×10^{11} (*D*). Stimulus intensity (in photons·cm^{-2}·s^{-1}) for P6: 7.30×10^8 (*A*), 2.28×10^{11} (*B*), 6.84×10^{11} (*C*), and 2.28×10^{12} (*D*). Stimulus intensity (in photons·cm^{-2}·s^{-1}) for P20: 2.28×10^8 (*A*), 2.28×10^9 (*B*), 7.30×10^9 (*C*), and 1.82×10^{12} (*D*).

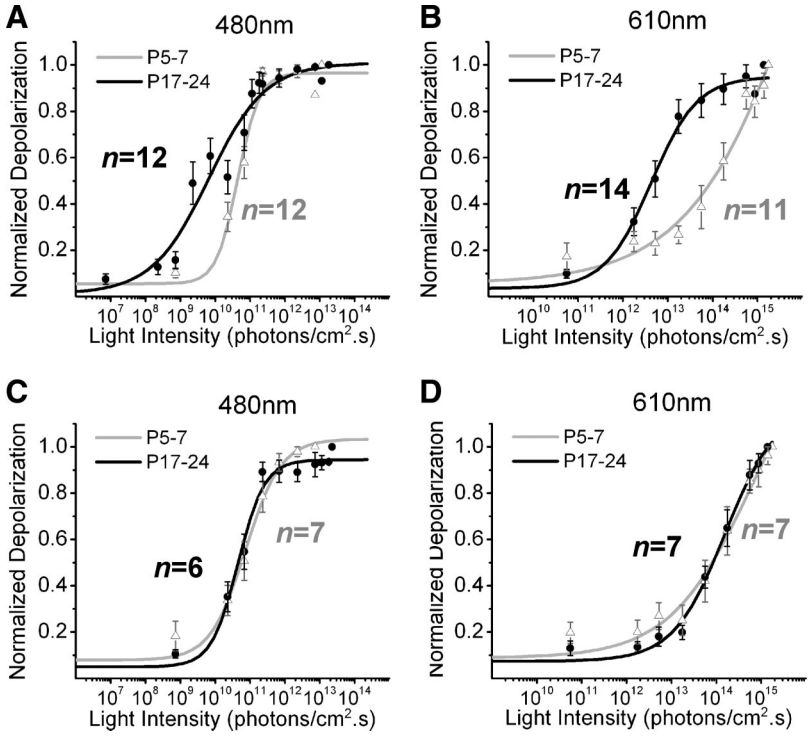

FIG. 6. Differences in sensitivity of light-evoked responses in P17–P24 and P5–P7 retinas. *A–D*: irradiance–response curves to 480- and 610-nm light in the absence (*A* and *B*) and presence (*C* and *D*) of glutamatergic synaptic blockers. Irradiance yielding half-maximal response (IR50) in photons·cm^{-2}·s^{-1} $IR50_{P17–P24} \cong 5.6 \times 10^9$, $IR50_{P5–P7} \cong 3.9 \times 10^{10}$ (*A*); $IR50_{P17–P24} \cong 3.5 \times 10^{12}$, $IR50_{P5–P7} \cong 7.9 \times 10^{13}$ (*B*); $IR50_{P17–P24} \cong 3.9 \times 10^{10}$, $IR50_{P5–P7} \cong 6.3 \times 10^{10}$ (*C*); $IR50_{P17–P24} \cong 7.9 \times 10^{13}$, $IR50_{P5–P7} \cong 7.9 \times 10^{13}$ (*D*).

ever, we would expect that ipRGCs at P5–P7 would have a λ_{max} of about 480 nm (Berson et al. 2002; Dacey et al. 2005) because spectral sensitivity of these cells is presumably determined only by the intrinsic system. To test this hypothesis, average light responses to increasing intensities of 610-nm light at P17–P24 and P5–P7 in the absence of synaptic blockers were normalized to averaged 480-nm responses within the same age group. We then estimated the λ_{max} for each group based on the differences in sensitivity to these two wavelengths (Lamb 1995). Indeed, we saw a shift in the λ_{max} from about 480 nm at P5–P7 to about 490 nm at P17–P24, demonstrating a shift in the spectral sensitivity of ipRGCs at adult stages to longer wavelengths, consistent with the idea that these cells are receiving midwavelength cone-driven input, in addition to being influenced by the intrinsic system.

Dendritic stratification and arborization of ipRGCs during development

The strong modulation of ipRGCs at adult stages due to synaptic inputs implies that these cells receive afferent connections from bipolar or amacrine cells in the IPL. A well-known developmental event in retinal maturation is the progressive segregation of RGC dendrites into the a and b sublaminas of the IPL, which is a morphological rearrangement crucial for the emergence of the ON and OFF pathways (Sernagor et al. 2001). We investigated whether ipRGC dendritic arborization and stratification in the IPL change throughout the first postnatal weeks of development. To examine how the stratification of ipRGC dendrites progresses from P0–P2 and P5–P7 to adult morphology we filled individual ipRGCs at P0–P2, P5–P7, or P17–P24 with either 0.5% biocytin or neurobiotin. We then utilized streptavidin conjugated with rhodamine to visualize the soma and dendritic processes of the biocytin/neurobiotin-filled cells. Retinas were also stained for choline acetyl transferase (ChAT), a marker of cholinergic amacrine cells in the GCL and in the INL. ChAT is expressed very early in retinal development (Stacy and Wong 2003) and its staining allowed us to visually identify the relative locations of the ON and OFF sublaminas of the IPL. At P0–P2 and P5–P7 it was difficult to visualize the different sublaminas of the IPL using the ChAT antibody staining, although it did appear that ipRGCs were monostratified at these ages (Fig. 7, *D* and *E*). Two distinct levels of stratification of ipRGC dendrites were seen at P17–P24, corresponding to stratification in the ON-(inner) and OFF-(outer) sublaminas. Examples of ipRGC stratification within the IPL, measured from 27 cells (P17–P24), are shown in Fig. 7, *A–C*. For one group of cells the dendrites stratified at the inner (ON) sublamina of the IPL, near the GCL (14/27 cells) (Fig. 7*B*). In a second group of cells the dendrites stratified at the outer borders of the IPL (OFF sublamina) near the INL (6/27 cells) (Fig. 7*A*). We also observed a third group of cells that displayed distinct stratification in both the inner (ON) and outer (OFF) sublaminas of the IPL (7/27 cells) (Fig. 7*C*). Three subtypes of ipRGCs were also described by Viney et al. (2007) using transynaptic viral tracing techniques in mice. Following their terminology, we found that in P17–P24 mice, about 22% of cells were type I with dendritic stratification restricted to the OFF sublamina in the IPL, about 52% of cells were type II with dendritic arborization restricted to the ON sublamina and about 26% of cells were type III with bistratified dendritic arbors in both the ON and OFF sublaminas. Quantification of dendritic field diameter and total dendritic length of the neurobiotin/biocytin-filled cells shows that there is an increase in dendritic field diameter [mean ± SE (in μm): P0–P2 = 107 ± 8; P5–P7 = 182 ± 53; P17–P24 = 339 ± 18] and total dendritic length [mean ± SE (in μm): P0–P2 = 976 ± 53; P5–P7 = 1,688 ± 142; P17–P24 = 3,337 ± 359] with age (Fig. 7*F*).

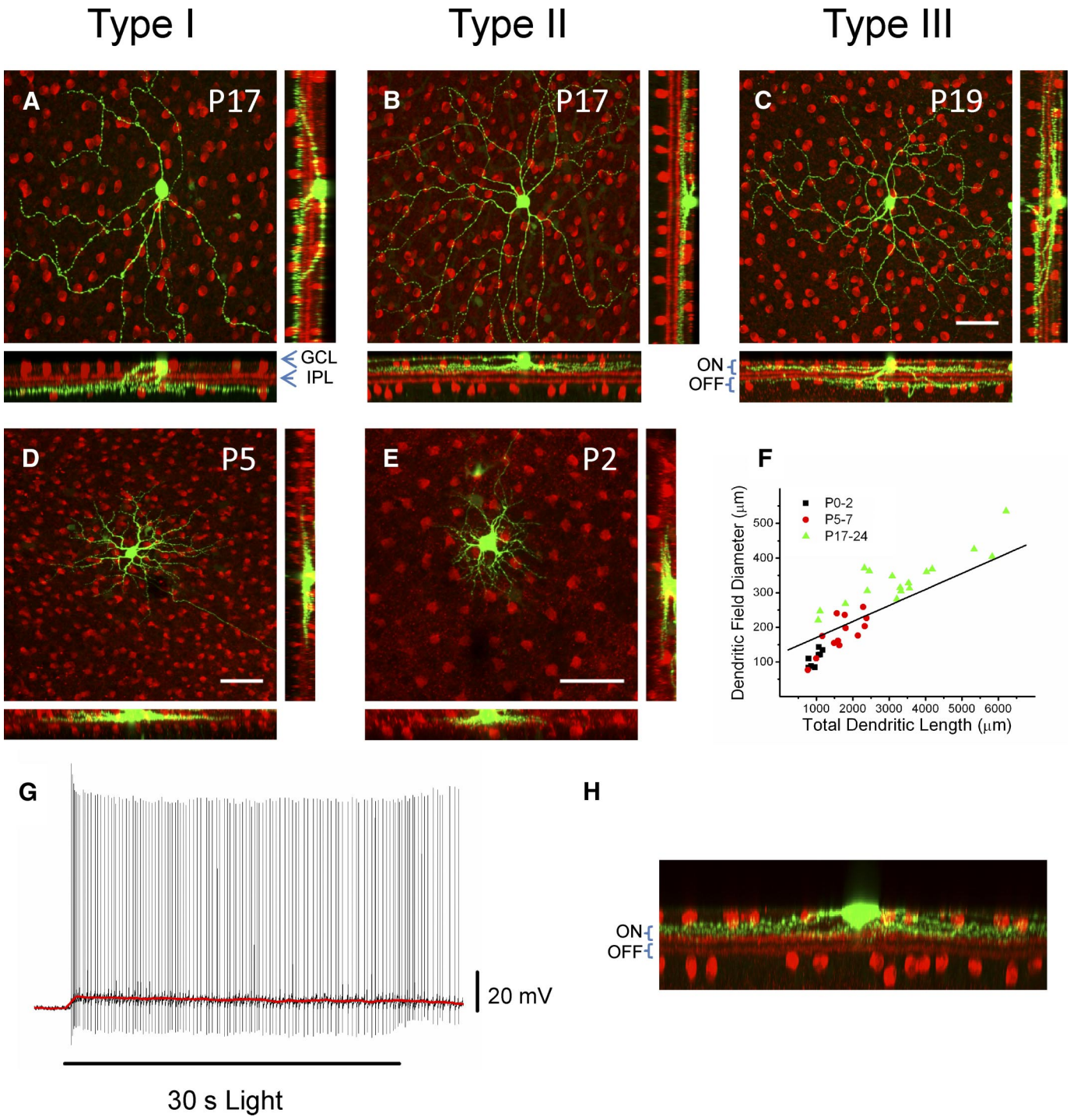

FIG. 7. Morphological diversity of ipRGCs during mouse development. Whole-mount retinas of ipRGCs filled with biocytin/neurobiotin (in green) and immunostained ChAT (in red) to visualize cholinergic amacrine cells (*A–E*). *Top row*: examples of 3 types of ipRGCs in P17–P24 mice. ChAT-positive cell bodies are in the GCL and the INL, whereas their projections form 2 bands visible in the rotated images that run along the ON and OFF sublamina of the IPL (*bottom* and *right panels* of *A–E*). *A*: monostratified ipRGC (P17) with dendritic arborization in the OFF sublamina of the IPL (type I ipRGC). *B*: monostratified ipRGC (P17) with dendritic arborization in the ON sublamina of the IPL (type II ipRGC). *C*: bistratified ipRGC (P19) with ON and OFF segregated arborization with respect to the 2 anti-ChAT–labeled bands (type III ipRGC). *D* and *E*: examples of ipRGC confocal images taken from P5 and P2 mice. *F*: dendritic length and dendritic field diameter of individual ipRGCs at P0–P2, P5–P7, and P17–P24. *G*: example of intrinsic light response (p53) of type II cell to a 30-s white-light stimulus recorded in current-clamp mode in the presence of synaptic blockers. Red line shows membrane potential values averaged over a 1-s sliding time window. *H*: dendritic stratification of cell from *G* in the ON sublamina of the IPL. ChAT, choline acetyl transferase; GCL, ganglion cell layer; IPL, inner plexiform layer. Scale bars: 50 μm for *A–E*.

Inner and outer stratifying ipRGCs in primates have both been found to be intrinsically photosensitive (Dacey et al. 2005). Although intrinsic photosensitivity has been confirmed in rodent type I (M1, outer-stratifying) ipRGCs (Berson et al. 2002), this has yet to be demonstrated directly in rodent type II (M2, inner-stratifying) ipRGCs (Baver et al. 2008; Hattar et al. 2006). To directly demonstrate intrinsic photosensitivity of type II ipRGCs in the mouse, we dye-filled EGFP-positive cells from adult (P53–P54) mice with neurobiotin and recorded light responses to a 30-s white-light stimulus in the presence of a cocktail of synaptic blockers (10 μM DNQX and 250 μM DL-AP4) to block signaling from the outer retina. We then coimmunostained for ChAT and performed immunocytochemistry as described earlier to determine the stratification subtype of the filled cell. By filling only one cell per preparation, we were able to directly correlate the light response of a given cell to its dendritic stratification subtype. As expected, type II cells responded to a 30-s white-light stimulus with a sluggish, sustained depolarization in the presence of synaptic blockers ($n = 5$), confirming the intrinsic photosensitivity of inner-stratifying, type II ipRGCs. Figure 7, *G* and *H* shows an example of the intrinsic light response and dendritic stratification of a single adult type II ipRGC.

DISCUSSION

The results of our study indicate that melanopsin-expressing ganglion cells undergo major functional remodeling during early postnatal development in mice. Although calcium imaging and multielectrode recordings of mouse retinas have indicated light responsiveness of ipRGCs during early neonatal stages, these studies have relied on various pharmacological blockers and knockout mice to isolate and compare their intrinsic light responses at early neonatal and adult stages (Sekaran et al. 2005; Tu et al. 2005). We used a novel transgenic mouse model to identify ipRGCs in situ, allowing for the electrophysiological recording of these cells in the absence of synaptic blockers. We followed the time course of development of synaptic connections onto these cells and we compared the "intrinsically" and "extrinsically" mediated light responses of ipRGCs during the developmental periods before and after eye opening in the mouse.

It was important to first validate the BAC transgenic mouse model in which expression of EGFP is driven by the melanopsin promoter. The fidelity of this reporter mouse line for melanopsin expression was demonstrated by: *1*) colocalization of EGFP and melanopsin expression in subpopulations of ganglion cells, *2*) lack of expression of EGFP in other tissues, and *3*) functional demonstration of intrinsic light responses in EGFP-positive cells. Overall, the intrinsic light responses recorded from EGFP-positive cells were similar to those previously described in rat and mouse ipRGCs identified using cell tracers or extracellular recordings (Berson et al. 2002; Hattar et al. 2002; Warren et al. 2006). In our experiments, under conditions in which synaptic influences from rods and cones were blocked pharmacologically, EGFP-positive cells sampled during the first three postnatal weeks of development displayed a slow and sustained depolarization on light stimulation, consistent with melanopsin phototransduction (Berson et al. 2002; Hattar et al. 2002; Warren et al. 2006).

With the ability to visually identify individual ipRGCs, we were able to record and fill these cells with the small-molecular-weight dye biocytin or neurobiotin. Morphological reconstructions of filled ipRGCs show that cells at P17–P24 have extensive dendritic arborization in the IPL ON and OFF sublaminas. We recognized three types of ipRGCs, the most frequent of which showed dendritic stratification restricted to the ON sublamina, another in which the dendrites terminated in the OFF sublamina, and another subpopulation in which the dendrites bistratified in both sublaminas. Likewise, there was a progressive increase in dendritic field size and complexity during the analyzed period. The synaptically driven depolarizing light responses at P17–P24 are consistent with the larger subpopulation of ipRGCs observed with dendrites terminating only in the ON sublamina. This is in contrast to findings in rat ipRGCs, in which it was reported that ipRGC dendrites terminate mainly in the OFF sublamina (Berson et al. 2002; Hattar et al. 2002). However, a recent study using transynaptic viral tracing in mice also found three distinctly stratifying ipRGC populations. This study found that the ON and OFF stratifications were equally predominant and that a smaller proportion of cells was ON–OFF stratified (Viney et al. 2007). Additionally, evidence from melanopsin knockout mice and from the use of antibody staining to the N and C termini of the melanopsin protein has identified at least two populations of distinctly stratifying ipRGCs within the retina termed M1 (which appear to stratify in the outer IPL, analogous to type I) and M2 (which may stratify only in the proximal IPL, analogous to type II) (Baver et al. 2008; Hattar et al. 2006). Baver et al. (2008) saw about 56% of ipRGCs staining as M1 (OFF-stratifying) and about 46% staining as M2 (ON-stratifying), whereas Viney et al. (2007) saw about 39% type I (OFF-stratifying), about 41% type II (ON-stratifying), and about 20% type II (ON–OFF bistratified). Our results are in support of three distinct types of dendritic stratification within the population of ipRGCs, similar to the findings of Viney et al. (2007), although we observed about 22% type I, 52% type II, and 26% type III. At this time, it is not clear what the source of discrepancy between proportion of dendritic stratification types seen in this study versus those of Baver et al. (2008) or Viney et al. (2007) could be. It is possible that ON-stratifying cells were somehow oversampled in our experimental system where EGFP-positive cells were selected at random for dye filling, whereas in other systems a large proportion of ipRGCs was labeled in bulk using viral tracing or antibody staining. ON- and OFF-stratifying ipRGCs have also been identified in primate retina, with OFF-stratifying cells being the predominant subtype (Dacey et al. 2005; Jusuf et al. 2007). Although two types of stratification have been identified in primate and demonstrated to be intrinsically photosensitive (Dacey et al. 2005), this study was the first to directly demonstrate intrinsic photosensitivity of type II melanopsin RGCs in the rodent, confirming the intrinsic photosensitivity of another morphological subtype of melanopsin-expressing RGCs. Perhaps the most intriguing aspect of these differences in stratification is the fact that, whereas individual ipRGCs clearly demonstrate specific segregation within different sublaminas of the IPL, adult ipRGCs appear to receive synaptically driven depolarization only at light on (Dacey et al. 2005). We did not observe the weak synaptically driven depolarization at light off reported by Wong et al. (2007), but this aspect of the response could be masked by the pronounced

repolarization we observed at the offset of the light stimulus. A careful analysis of the specific types of synaptic connections onto each of these ipRGC morphological subtypes, as well as an analysis of any differences in their intrinsic responses, will be a necessary next step in characterizing the different morphological subtypes of ipRGCs.

This study was the first to follow the developmental time course of the emergence of functional signaling from the outer retina to ipRGCs. Perhaps the major finding in this study was that photoresponses of ipRGCs changed dramatically between the periods before and after eye opening. By the second postnatal week (P11–P14), synaptically driven light responses evoked by cone/rod pathways were already detected in ipRGCs using whole cell current-clamp recordings. This is consistent with research on development of the image-forming visual system, which has shown that functional synaptic connectivity between ganglion cells and the outer retina is first detectable around the time of eye opening (Sernagor et al. 2001), demonstrating that in this case, the image- and nonimage-forming visual pathways do develop with a similar time course. At least in our experiments, in which the retinas were partially light adapted (see METHODS), we noticed that by the third postnatal week, almost all ipRGCs depolarized with a markedly accelerated onset and offset to light stimulus in contrast to the slower response kinetics observed in the first postnatal week of development. There was also a gain of sensitivity of about one log unit of irradiance for both 480 and 610 nm at later developmental stages (P17–P24). The fact that almost all ipRGCs at P17–P24 responded to light with cone/rod-mediated depolarization suggests that a synaptically driven influence is a general property of these cells. Perez-Leon et al. (2006), using whole cell voltage-clamp recordings, observed only about 5% of ipRGCs exhibiting synaptically driven light responses. In contrast, Wong et al. (2007), using multielectrode recording techniques, found that virtually every ipRGC exhibited a synaptically mediated light response. Our results indicate that at adult stages the ipRGCs are signaling to various brain areas via a summation of the "intrinsic" slow response and "extrinsic" fast response originating from outer retinal pathways. It is important to note that our recordings were performed at room temperature and this should be taken into account when comparing quantitative measurements of light responses in this study to those in studies in which recordings were done at more physiological temperatures.

In this mouse line, EGFP is presumably expressed in the entire population of ipRGCs that innervate various nonimage-forming central structures such as the SCN, pretectum, and the intergeniculate leaflet (Hattar et al. 2006). This idea is supported by the strong colocalization of EGFP and melanopsin expression. The relatively homogeneous and consistent synaptically mediated light responses in ipRGCs argue against the notion that these cells convey irradiance signals to the SCN with sluggish depolarization kinetics and with maximal spectral sensitivity centered at 480 nm (Berson 2003). Instead, the properties of ipRGC responses observed in early adult animals (P17–P24) are remarkably similar to those seen in the melanopsin-expressing cells of primates that project to the lateral geniculate nucleus and pretectal olivary nucleus (Dacey et al. 2005). Medium- and long-wavelength cones provide strong excitatory inputs to these ipRGCs providing spectral sensitivity and kinetics to light responses distinct from those provided by the melanopsin system (Dacey et al. 2005).

Because we used 480-nm light for EGFP detection, we performed electrophysiological recordings in retinas that were partially light adapted, thus reducing or even eliminating any contribution of the rods to the ipRGC extrinsic light response. The dynamic range of the photoresponses in the absence of synaptic blockers with 610 nm is in the range of 10^{11} to 10^{14} photons$\cdot$cm$^{-2}\cdot$s^{-1}, consistent with synaptically driven light responses mediated by cones, most likely of the medium-wavelength subtype. A recent report using a mouse model of medium-wavelength cone degeneration found that these photoreceptors have a significant role in circadian entrainment (Dkhissi-Benyahya et al. 2007). Our findings that synaptic inputs are conferring on ipRGCs an overall higher sensitivity to light, as well as shifting the λ_{max} of these cells from about 480 nm toward that of medium-wavelength cones, are in agreement with this idea. These results thus indicate an important role of medium-wavelength cones in providing light responsiveness to ipRGCs, and the shift in λ_{max} for adult ipRGCs to about 490 nm more closely matches the λ_{max} of about 500 nm reported for phase shifting in hamsters (Takahashi et al. 1984) and the λ_{max} of about 510 nm reported for SCN neurons in rat under photopic conditions (Aggelopoulos and Meissl 2000). This reinforces the notion that cone photoreceptors have an important contribution to nonimage-forming light responses in mammalian organisms.

The exclusive reliance of ipRGCs on melanopsin-mediated phototransduction at earlier stages (P0–P11) seems to indicate a lesser need at this developmental period for the distinct spectral tuning and kinetics provided by the cone/rod pathways. The suggested role of the cone/rod pathways in providing better discrimination of spectral changes at dawn and dusk (Panda 2007) and therefore stronger synchronization of the circadian clock may not be as relevant at mouse early newborn stages before eye opening, at a time when maternal care is provided on an almost full-time basis. However, global detection of irradiance levels by the melanopsin system might still be physiologically relevant even at early developmental stages to convey signals related to the sleep–wake cycle and hormonal regulation. Indeed, it is possible to induce c-Fos expression in the SCN of neonatal mice in vivo by exposing rat and mouse pups to light, implying a potential role for photoentrainment of the circadian clock even at early ages (Hannibal and Fahrenkrug 2004; Lupi et al. 2006). Another possible role for irradiance detection by the melanopsin system at early developmental stages is that light responses of ipRGCs may subserve an important role in driving the overall network activity of the inner retina by consolidating the development of RGCs (Sernagor 2005). Appropriate targeting of RGC axons during retinal development relies on activity-dependent refinement and consolidation of connections (Wong 1999). Several studies have indicated that RGC activity also plays a crucial role in the formation of visual cortex organization and in the stratification of RGC dendrites (Sernagor et al. 2001). To what extent ipRGCs contribute to the waves of depolarization before eye opening is presently unknown, but their ability to detect light at these early postnatal stages (albeit with low sensitivity, about 10^{10} to 10^{12} photons$\cdot$cm$^{-2}\cdot$s^{-1} for 480 nm at P0–P7) leaves open the possibility that these cells are somehow involved in the specific targeting and dendritic arborization that are occurring during this time period.

The development of this EGFP reporter mouse has also allowed us to measure the intrinsic membrane properties of these cells at early ages, something that is not possible using the extracellular techniques that have been used previously. The finding that membrane capacitance is significantly decreased in the presence of the gap-junctional blocker MFA at P5–P7, P11–P14, and P17–P24 is consistent with the idea that ipRGCs are electrically coupled during these periods. Indeed, these results are in agreement with previous reports, using calcium imaging or multielectrode array, of correlated firing between ipRGCs and other ganglion cells at P5–P10 (Sekaran et al. 2005; Tu et al. 2005). Prior to this study, Sekaran et al. (2003) reported, using calcium imaging in *rd/rd cl* mice, that adult ipRGCs were coupled and that this coupling could be blocked using carbenoxelone. Our data in P17–P24 mice in which the rods and cones are still intact provides additional evidence of coupling between adult ipRGCs. Interestingly, Tu et al. (2005), using multielectrode recordings in *rd/rd* mice, did not find any correlated firing in adult retinas. It remains to be determined to which types of cells ipRGCs are coupling and whether this coupling remains constant or changes during development.

Overall, our findings reveal marked developmental changes of ipRGCs in the mouse retina during a period in which neuronal differentiation, synaptogenesis, and cell death are all occurring with high frequency. Morphological expansion of ipRGC dendrites and their subsequent specific stratification in the inner plexiform layer is accompanied by the formation of functional connectivity with vertical pathways from the cone/rod systems. As development progresses, ipRGCs transition from being driven solely by intrinsic light responses to forming functional connections with vertical pathways from the cone/rod systems while still retaining their intrinsic photosensitivity. Such changes may reflect distinct roles for these cells at different time points throughout retinal development.

ACKNOWLEDGMENTS

We thank D. Hang and S. Liu for excellent technical assistance and Dr. Ignacio Provencio for providing the melanopsin antisera.

GRANTS

This work was supported in part by National Eye Institute Grants R01-EY-012949 and R21-EY-018885, University of Minnesota Graduate School, and McKnight Foundation.

REFERENCES

Aggelopoulos NC, Meissl H. Responses of neurones of the rat suprachiasmatic nucleus to retinal illumination under photopic and scotopic conditions. *J Physiol* 523: 211–222, 2000.

Baver SB, Pickard GE, Sollars PJ, Pickard GE. Two types of melanopsin retinal ganglion cell differentially innervate the hypothalamic suprachiasmatic nucleus and the olivary pretectal nucleus. *Eur J Neurosci* 27: 1763–1770, 2008.

Belenky MA, Smeraski CA, Provencio I, Sollars PJ, Pickard GE. Melanopsin retinal ganglion cells receive bipolar and amacrine cell synapses. *J Comp Neurol* 460: 380–393, 2003.

Berson DM. Strange vision: ganglion cells as circadian photoreceptors. *Trends Neurosci* 26: 314–320, 2003.

Berson DM. Phototransduction in ganglion-cell photoreceptors. *Pfluegers Arch* 454: 849–855, 2007.

Berson DM, Dunn FA, Takao M. Phototransduction by retinal ganglion cells that set the circadian clock. *Science* 295: 1070–1073, 2002.

Dacey DM, Liao HW, Peterson BB, Robinson FR, Smith VC, Pokorny J, Yau KW, Gamlin PD. Melanopsin-expressing ganglion cells in primate retina signal colour and irradiance and project to the LGN. *Nature* 433: 749–754, 2005.

Dkhissi-Benyahya O, Gronfier C, De Vanssay W, Flamant F, Cooper HM. Modeling the role of mid-wavelength cones in circadian responses to light. *Neuron* 53: 677–687, 2007.

Fu Y, Liao HW, Do MT, Yau KW. Non-image-forming ocular photoreception in vertebrates. *Curr Opin Neurobiol* 15: 415–422, 2005a.

Fu Y, Zhong H, Wang MH, Luo DG, Liao HW, Maeda H, Hattar S, Frishman LJ, Yau KW. Intrinsically photosensitive retinal ganglion cells detect light with a vitamin A-based photopigment, melanopsin. *Proc Natl Acad Sci USA* 102: 10339–10344, 2005b.

Hannibal J, Fahrenkrug J. Melanopsin containing retinal ganglion cells are light responsive from birth. *Neuroreport* 15: 2317–2320, 2004.

Hastings MH, Herzog ED. Clock genes, oscillators, and cellular networks in the suprachiasmatic nuclei. *J Biol Rhythms* 19: 400–413, 2004.

Hastings MH, Reddy AB, Maywood ES. A clockwork web: circadian timing in brain and periphery, in health and disease. *Nat Rev* 4: 649–661, 2003.

Hattar S, Kumar M, Park A, Tong P, Tung J, Yau KW, Berson DM. Central projections of melanopsin-expressing retinal ganglion cells in the mouse. *J Comp Neurol* 497: 326–349, 2006.

Hattar S, Liao HW, Takao M, Berson DM, Yau KW. Melanopsin-containing retinal ganglion cells: architecture, projections, and intrinsic photosensitivity. *Science* 295: 1065–1070, 2002.

Herzog ED. Neurons and networks in daily rhythms. *Nat Rev* 8: 790–802, 2007.

Jusuf PR, Lee SC, Hannibal J, Grunert U. Characterization and synaptic connectivity of melanopsin-containing ganglion cells in the primate retina. *Eur J Neurosci* 26: 2906–2921, 2007.

Kumbalasiri T, Provencio I. Melanopsin and other novel mammalian opsins. *Exp Eye Res* 81: 368–375, 2005.

Lamb TD. Photoreceptor spectral sensitivities: common shape in the long-wavelength region. *Vision Res* 35: 3083–3091, 1995.

Lee YT, Wang Q. Inhibition of hKv2.1, a major human neuronal voltage-gated K^+ channel, by meclofenamic acid. *Eur J Pharmacol* 378: 349–356, 1999.

Lucas RJ, Hattar S, Takao M, Berson DM, Foster RG, Yau KW. Diminished pupillary light reflex at high irradiances in melanopsin-knockout mice. *Science* 299: 245–247, 2003.

Lupi D, Sekaran S, Jones SL, Hankins MW, Foster RG. Light-evoked FOS induction within the suprachiasmatic nuclei (SCN) of melanopsin knockout (Opn4−/−) mice: a developmental study. *Chronobiol Int* 23: 167–179, 2006.

Maywood ES, O'Neill J, Wong GK, Reddy AB, Hastings MH. Circadian timing in health and disease. *Prog Brain Res* 153: 253–269, 2006.

Metea MR, Newman EA. Glial cells dilate and constrict blood vessels: a mechanism of neurovascular coupling. *J Neurosci* 26: 2862–2870, 2006.

Muyrers JP, Zhang Y, Testa G, Stewart AF. Rapid modification of bacterial artificial chromosomes by ET-recombination. *Nucleic Acids Res* 27: 1555–1557, 1999.

Newman EA, Bartosch R. An eyecup preparation for the rat and mouse. *J Neurosci Methods* 93: 169–175, 1999.

Pan F, Mills SL, Massey SC. Screening of gap junction antagonists on dye coupling in the rabbit retina. *Vis Neurosci* 24: 609–618, 2007.

Panda S. Multiple photopigments entrain the mammalian circadian oscillator. *Neuron* 53: 619–621, 2007.

Peirson S, Foster RG. Melanopsin: another way of signaling light. *Neuron* 49: 331–339, 2006.

Peretz A, Degani N, Nachman R, Uziyel Y, Gibor G, Shabat D, Attali B. Meclofenamic acid and diclofenac, novel templates of KCNQ2/Q3 potassium channel openers, depress cortical neuron activity and exhibit anticonvulsant properties. *Mol Pharmacol* 67: 1053–1066, 2005.

Perez-Leon JA, Warren EJ, Allen CN, Robinson DW, Lane Brown R. Synaptic inputs to retinal ganglion cells that set the circadian clock. *Eur J Neurosci* 24: 1117–1123, 2006.

Sekaran S, Foster RG, Lucas RJ, Hankins MW. Calcium imaging reveals a network of intrinsically light-sensitive inner-retinal neurons. *Curr Biol* 13: 1290–1298, 2003.

Sekaran S, Lupi D, Jones SL, Sheely CJ, Hattar S, Yau KW, Lucas RJ, Foster RG, Hankins MW. Melanopsin-dependent photoreception provides earliest light detection in the mammalian retina. *Curr Biol* 15: 1099–1107, 2005.

Sernagor E. Retinal development: second sight comes first. *Curr Biol* 15: R556–R559, 2005.

Sernagor E, Eglen SJ, Wong RO. Development of retinal ganglion cell structure and function. *Prog Retinal Eye Res* 20: 139–174, 2001.

Takahashi JS, DeCoursey PJ, Bauman L, Menaker M. Spectral sensitivity of a novel photoreceptive system mediating entrainment of mammalian circadian rhythms. *Nature* 308: 186–188, 1984.

Tu DC, Zhang D, Demas J, Slutsky EB, Provencio I, Holy TE, Van Gelder RN. Physiologic diversity and development of intrinsically photosensitive retinal ganglion cells. *Neuron* 48: 987–999, 2005.

Viney TJ, Balint K, Hillier D, Siegert S, Boldogkoi Z, Enquist LW, Meister M, Cepko CL, Roska B. Local retinal circuits of melanopsin-

containing ganglion cells identified by transynaptic viral tracing. *Curr Biol* 17: 981–988, 2007.

Warren EJ, Allen CN, Brown RL, Robinson DW. Intrinsic light responses of retinal ganglion cells projecting to the circadian system. *Eur J Neurosci* 17: 1727–1735, 2003.

Warren EJ, Allen CN, Brown RL, Robinson DW. The light-activated signaling pathway in SCN-projecting rat retinal ganglion cells. *Eur J Neurosci* 23: 2477–2487, 2006.

Wong KY, Dunn FA, Graham DM, Berson DM. Synaptic influences on rat ganglion-cell photoreceptors. *J Physiol* 582: 279–296, 2007.

Wong RO. Retinal waves and visual system development. *Annu Rev Neurosci* 22: 29–47, 1999.

Yang XW, Model P, Heintz N. Homologous recombination based modification in Escherichia coli and germline transmission in transgenic mice of a bacterial artificial chromosome. *Nat Biotechnol* 15: 859–865, 1997.